PCCP

Two-Photon Chemistry of Tetrahydrofuran in Clathrate Hydrates

Journal:	*Physical Chemistry Chemical Physics*
Manuscript ID	CP-ART-06-2023-002607.R2
Article Type:	Paper
Date Submitted by the Author:	09-Oct-2023
Complete List of Authors:	Michon, Michael; Brown University Chmielniak, Pawel; Brown University Weber, Peter; Brown University Rose-Petruck, Christoph; Brown University

SCHOLARONE™
Manuscripts

PAPER

Two-Photon Chemistry of Tetrahydrofuran in Clathrate Hydrates

Received 00th May 2023,
Accepted 00th May 2023

DOI: 10.1039/x0xx00000x

Michael A. Michon,*[a] Pawel Chmielniak,[a] Peter M. Weber*[abd] and Christoph Rose-Petruck*[acd]

High-lying electronic states hold the potential for new and unusual photochemical reactions. However, for conventional single-photon excitation in the condensed phase, reaching these states is often not possible because the vacuum-ultraviolet (VUV) light required is competitively absorbed by the surrounding matrix rather than the molecule of interest. Here, this hurdle is overcome by leveraging nonresonant two-photon absorption (2PA) at 265 nm to achieve preferential photolysis of tetrahydrofuran (THF) trapped within a clathrate hydrate network at 77 K. Electron spin resonance (ESR) spectroscopy enables direct observation and identification of otherwise short-lived organic radicals stabilized by the clathrate cages, providing clues into the rapid dynamics that immediately follow photoexcitation. 2PA induces extensive fragmentation of enclathrated THF yielding 1-alkyl, acyl, allyl and methyl radicals—a stark departure from the reactive motifs commonly reported in *γ*-irradiated hydrates. We speculate on the undetected transient dynamics and explore the potential role of trapped electrons generated from water and THF. This demonstration of nonresonant two-photon chemistry presents an alternative approach to targeted condensed phase photochemistry in the VUV energy range.

1 Introduction

The vast majority of photochemical reactions studied are induced by the absorption of a single photon. Since most materials absorb light in the far-UV and VUV range of the spectrum, conventional photochemistry in condensed phase systems is restricted to reactions induced by excitation of molecules to their lowest excited electronic states. Even water, which is exceptionally transparent in the UV, absorbs strongly at wavelengths below 175 nm (Fig. 1a). Consequently, for most applications outside of the gas phase, one cannot selectively prepare a molecule of interest in one of its many higher excited states. This hinders the study of a large number of electronic states that, because of their high energy and the nature of the potential energy surfaces, might be involved in unique and useful photochemical reactions in systems where outcomes are strongly influenced by rapid vibrational energy redistribution to the surroundings. While this limitation can sometimes be side-stepped by employing sequential resonant excitations at longer wavelengths, this approach necessitates the existence of a short-lived, lower-lying intermediate state to "piggyback" off.[1,2] However, inefficient excited state absorption from this intermediate state could result in a sub-population of molecules undergoing spurious dynamics that complicate the analysis and obfuscate the chemistry under

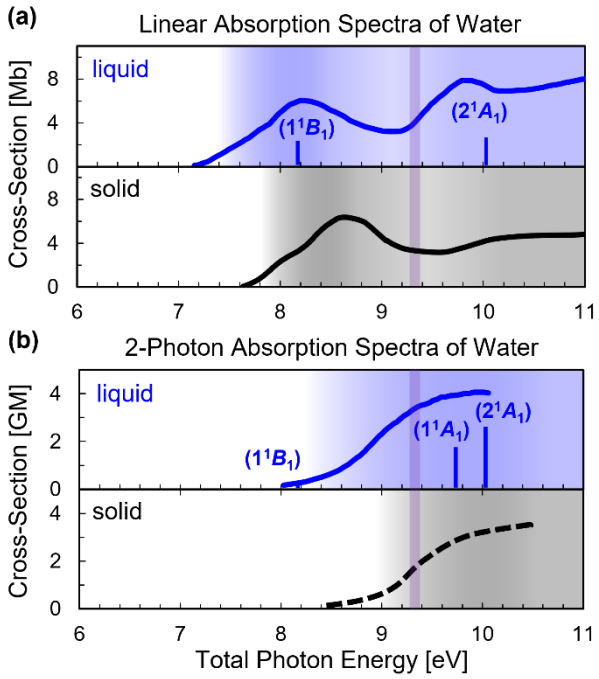

Figure 1: One- **(a)** and two-photon **(b)** absorption spectra of water in its liquid[29,30] (blue) and solid[31] (black) phases, solid curves, from the literature. The dashed black line illustrates a hypothetical 2PA spectrum of water ice which has yet to be reported. The absorption spectrum of water making up a clathrate hydrate is expected to correspond roughly to that of ice Ih due to the strong structural similarities between these two phases. The energies, relative oscillator strengths, and 2PA cross-sections (×40 GM) calculated for the lowest lying electronic states in liquid water[32] are indicated by vertical blue bars. Note the parity-induced weakening of the HOMO-LUMO transition 1^1B_1 in the 2PA spectrum extending the transparency window. The vertical purple bar indicates the total energy of two 265 nm photons (9.36 eV) lies near the anticipated onset of 2PA of water in clathrate hydrates.

[a] Department of Chemistry, Brown University, Providence, Rhode Island 02912
[b] peter_weber@brown.edu
[c] crosepet@brown.edu
[d] Authors contributed equally

Electronic Supplementary Information (ESI) available: [details of any supplementary information available should be included here]. See DOI: 10.1039/x0xx00000x

study. Furthermore, the specific energies of these resonances will often restrict the experimenter to more elaborate nondegenerate ("two-color") excitation schemes which require precise timing of multiple tunable ultrafast light sources.[3–6] In contrast, *nonresonant* two-photon absorption (2PA) is a third-order non-linear optical process ($\chi^{(3)}$) involving the *simultaneous* absorption of a pair of photons by a material (one that is normally transparent at the chosen wavelength) mediated by a virtual state.[7,8] This strategy not only preserves the dynamics resulting from direct excitation but also grants access to new electronic states that are forbidden by one-photon selection rules while weakening others.[9] In degenerate ("one-color") 2PA, both photons are delivered by the same laser beam, greatly simplifying the experimental implementation for use in widely accessible ultrafast light sources.[10,11] The distinct intensity dependence of 2PA has led to many applications, including but not limited to 3D lithography,[12,13] microscopy,[14,15] and therapeutics,[16] using near-IR lasers. In the target system, we employ 2PA to achieve direct photolysis of organic molecule guests embedded in an aqueous host matrix while mitigating competitive absorption by water. The enhanced transparency of water (Fig. 1b) is granted by the distinct selection rules of 2PA. While this two-photon chemistry (2PC) need not be strictly limited to aqueous matrices, the cavities of clathrate hydrates are highly effective at stabilizing the photochemically produced radicals nearly indefinitely[17–39] making them amenable to observation by spectroscopic methods with inherently low time resolution such as electron spin resonance (ESR).

Clathrate hydrates are host-guest inclusion compounds consisting of a fully saturated H-bonded network of water molecules with cavities that can accommodate a wide variety of small molecules.[40] THF promotes the growth of structure-II (sII) hydrates which have a cubic unit cell consisting of 136 H_2O molecules occupying the vertices of 16 small and 8 large polyhedral cages with hydrogen bonds directed along the edges. THF exclusively occupies the large, hexadecahedral cages, consisting of 12 pentagonal faces and 4 hexagonal faces ($5^{12}6^4$) while the 8 small, dodecahedral cages (5^{12}) remain empty. Crystalline growth of stoichiometric THF hydrates[§] can be nucleated from an aqueous solution at ~4.4 °C and ambient pressure.[41–43] The stability of enclathrated radicals is attributed to the strong H-bonding of the host and their comparatively weak Van der Waals interactions with the guests.[44] In this work, we extend the use of 2PA with UV pulses to condensed phase chemistry and explore the two-photon induced photolysis of an organic molecule, tetrahydrofuran (THF, C_4H_8O), encapsulated within the clathrate hydrate framework.

2 Results and Discussion

To estimate the relative contributions of water and THF to 2PA in the binary system proper, the non-linear response of each neat liquid was measured at 265 nm. Next, stoichiometric THF hydrates[§] grown from 5.88 mol% aqueous solutions were irradiated at 77 K to produce several different enclathrated organic radical species. The identities of these radicals, as revealed by steady-state ESR spectroscopy, point to a formation mechanism involving extensive fragmentation of the THF molecule[45] and support the notion that this process is initiated by a direct electronic excitation of THF without any meaningful participation from water. Finally, we form a hypothesis, one consistent with our observations and literature precedent, regarding the nature of the fast dynamic not probed in the present study.

2.1 Nonlinear Optical Responses

Neither water nor THF exhibit linear absorption at 265 nm.[46–48] Therefore, any nonlinear optical response must be attributed, at least in part, to 2PA. To assess the transparency of water under high intensity radiation at 265 nm (3rd harmonic of the Ti:sapphire laser) and the photoselectivity towards THF in the clathrate hydrate, it is important to determine the intrinsic 2PA cross-sections δ of both components at this wavelength. This in principle can be accomplished with several intensity dependent transmittance measurement schemes,[49] however, there are practical challenges associated with growing an optically transparent clathrate hydrate single-crystal of uniform thickness and presenting it to the laser while maintaining thermodynamic stability. One would then need to disentangle the contribution of both components from the total transmittance. As a proxy, the transmittance of the focused pump light through 1 cm neat liquid samples of water and THF was measured at ambient temperature as a function of incident peak intensity (Fig. 2). Attenuation of the incident light due to absorption in the 1 mm quartz windows of the sample cuvette was corrected for using an analogous measurement on just one such window in isolation. 2PA coefficients β were obtained by fitting the transmittance measurements to a theoretical model of 2PA[49] (Equations 1-4 in Methods) and the best fit values are reported in Table 1.

The measured transmittance of liquid water (blue points) serve primarily as a benchmark for validating the experimental setup as β_{H2O} is well-reported in the literature near 265 nm.[50–52] A fit to the 2PA model (blue line) gives $\beta_{H2O} = 5.6(\pm0.1)\times10^{-12}$ m/W, which is nearly within the uncertainty range of the value $4.9(\pm0.5)\times10^{-12}$ m/W reported by Dragonmir *et al*. at 264 nm.[50] Considering the high degree of variability found between such measurements throughout the literature, the level of quantitative agreement seen here for liquid water lends confidence to the experimental design.

The measured transmittance of liquid THF (red points) fits well to the theoretical model at peak intensities below ~6 GW/cm^2 but then is overestimated above this threshold. The deviations are likely due to the appearance of higher order, $\chi^{(>3)}$ nonlinear optical effects such as three-photon absorption (3PA) and two-photon induced excited state absorption (ESA) at elevated intensities. The open points in this high-intensity regime were thus excluded from the fit in order to obtain an estimate of $\beta_{THF} = 16.8(\pm2.0)\times10^{-12}$ m/W. From these measurements, we conclude that δ_{THF} exceeds δ_{H2O} by a factor of 14 ± 2 at 265 nm. This is consistent with the earlier onset of 2PA in THF measured at 355 nm ($2\hbar\omega$ = 7 eV) to be $4(\pm1)\times10^{-12}$ m/W compared to < 0.1×10^{-12} m/W in water.[53] Given the 1:17 molar ratio of THF to water in the stoichiometric sII clathrate hydrate,[§] their relative contributions to 2PA in the binary phase would be

 This journal is © The Royal Society of Chemistry 2023

Please do not adjust margins

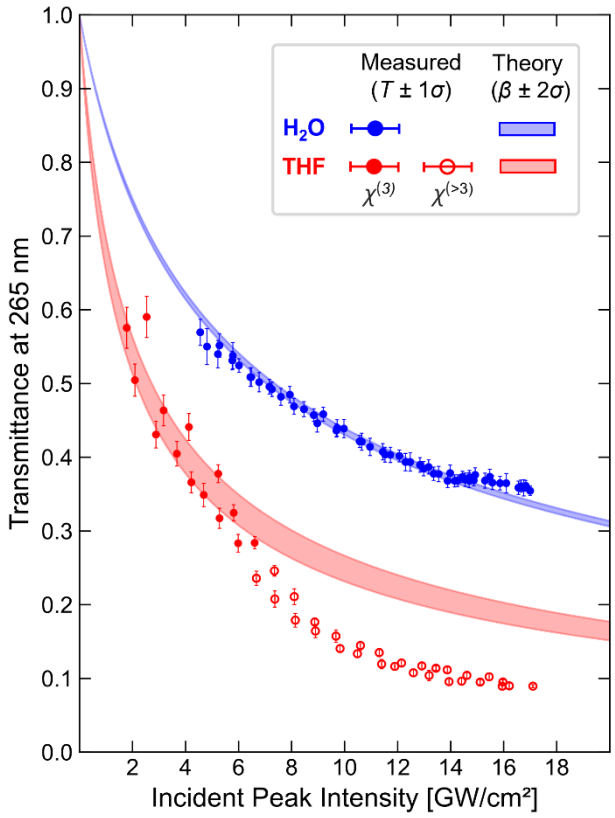

Figure 2: Transmittance of the focused 265 nm pump laser through 1 cm liquid samples of water (blue) and THF (red) as a function of incident peak intensity. The points are the measured transmittance with ± 1σ error bars. The solid curves are simulated fits to the filled data points using a simple theoretical model of 2PA (see Methods) where the shaded regions are bound by ± 2σ in the fit parameter β. The red, open data points could not be adequately described by the 2PA model alone and were thus excluded from the fit for THF. The observed deviation from the theory is likely due to an increasing contribution of $\chi^{(>3)}$ nonlinear effects at high intensity.

approximately $1\delta_{THF}/17\delta_{H2O}$ = 0.8 ± 0.1 assuming that their respective 2PA cross-sections do not change substantially from the liquid. However, δ_{H2O} at 265 nm for both ice and hydrate phases is expected to decrease with respect to liquid water due to strong perturbations induced by their fully coordinated, tetrahedral H-bond networks on the upper $4a_1$ Rydberg orbital[9] common to both 1^1B_1 and 2^1A_1 transitions (note the blue-shift of their associated features for the solid in Fig. 1a). Therefore, we expect nearly equal participation in 2PA between the two components of the THF hydrate, despite the 17-fold disparity in their concentrations. In the next section, we will see that the formation of all photoproducts detected following UV irradiation are best explained by preferential 2PA by THF rather than by two-photon ionization and dissociation of water.

Table 1: 2PA coefficients (β) and cross-sections δ for liquid water and THF measured at 265 nm. Parameters were extracted from fits to the 2PA model (Eqns. 1-4) and given ± 2σ error bars. δ are reported in units of "Goeppert-Mayer" where 1 GM = 10^{-58} m^4s/photon.

Liquid Sample	β ×10^{12} [m/W]	δ [GM]
H_2O	5.6 ± 0.1	1.25 ± 0.03
THF	16.8 ± 2.0	17.0 ± 2.1

2.2 Nonlinear Photochemical Response

Three varieties of isotopically labelled THF hydrates were exposed to high intensity 265 nm laser radiation at 77 K for 2 hours. Afterwards, the hydrate-stabilized radicals produced were detected using ESR spectroscopy. Dramatic attenuation of the pump laser due to scattering in the snow-like cryogenic samples necessitated the use of tighter focal conditions, long irradiation times, and a helical scan pattern to generate enough radicals for adequate signal-to-noise. Figure 3 features the ESR spectra of fully deuterated (top), host deuterated (middle), and guest deuterated (bottom) THF clathrate hydrates following UV irradiation. These spectra all possess sharp, isotropic features characteristic of highly disordered radical guests stably residing within clathrate cages.[54,55] By contrast, control measurements of the irradiated pure solvent constituents differ considerably from the hydrate spectra, instead sporting weak, broad features with high anisotropy (Fig. S11). The origins and identities of several different radical species can be deduced from these spectra and a detailed characterization of each is presented in SI.3.

In the field range between 338-352 mT with g-factors close to that of the free-electron (2.0023) are signals related to organic, carbon-centered radicals (Fig. 3c). A full basis analysis of the ESR spectrum presented in Figure 4 reveals at least four distinct species that constitute the signal in this region. Most prominent among these, present in all samples containing undeuterated THF, is a "triple-triplet" characteristic of a 1-alkyl radical. Variable temperature ESR measurements corroborate this assignment (Figs. S13-14); the hyperfine coupling (HFC) interaction associated with one pair of protons in this radical shows a strong temperature dependence while the interaction with the other pair remains constant. This behavior is explained as thermal averaging due to unhindered rotation of a terminal methylene carrying the unpaired spin density (Fig. S14b). The denser, unresolved splitting pattern in the ESR spectrum of the d8-THF hydrate is indeed a "quintuple-quintet" produced by a deuterated 1-alkyl radical (Fig. S10). This species could only have formed from ring-opening or fragmentation of the THF molecule through the breakage of C-O or C-C bonds:

$$\mathrm{THF} \xrightarrow{2\times 265\ \mathrm{nm}} \mathrm{RCH_2CH_2^{\bullet}} + \mathrm{R'} \qquad \textbf{(1)}$$

There is some level of ambiguity regarding the identity of the R-groups since there are multiple sites where ring-cleavage could occur, and with the spin density is localized primarily on the terminal carbon, ESR cannot probe the molecular structure beyond the second carbon atom. Regardless, the formation of any 1-alkyl radical strongly points to the direct two-photon photolysis of THF which strongly contrasts with the typical radical formation mechanisms seen in γ-ray[19–25,28] or MeV proton[35] irradiated hydrates. In such studies, water molecules from the host framework absorb the brunt of the radiation and are split into atomic hydrogen ($H^{\bullet}$) and hydroxyl ($OH^{\bullet}$) radicals:

$$\mathrm{H_2O} \xrightarrow{\gamma\text{-ray}} \mathrm{H^+ + e^- + OH^{\bullet}} \longrightarrow \mathrm{H^{\bullet} + OH^{\bullet}} \qquad \textbf{(2)}$$

Please do not adjust margins

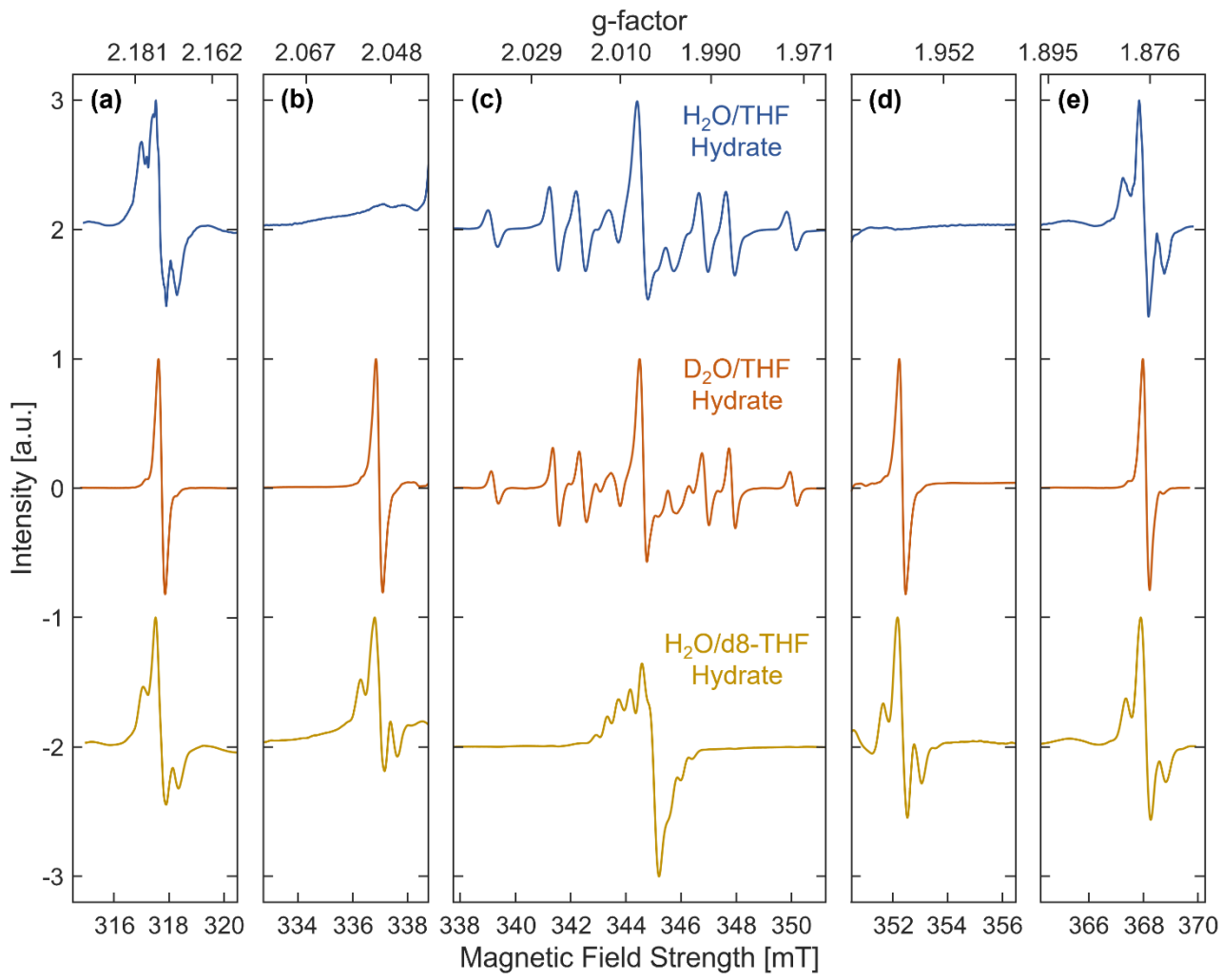

Figure 3: ESR spectra of irradiated, isotopically labelled THF clathrate hydrates at 77 K. H_2O/THF hydrate (top), D_2O/THF hydrate (middle), and H_2O/d8-THF hydrate (bottom). The signatures of atomic **(a)/(e)** hydrogen and **(b)/(d)** deuterium radicals at low-/high-field respectively. Between these **(c)** is a superposition of signals corresponding to organic radical fragments originating from THF. A full decomposition of these spectra into a basis of assigned radical components is presented in Figure 4. The spectra in each subplot are normalized over a common field range to provide a clear comparison.

The products of water splitting (particularly $OH^\bullet$) then scavenge H atoms from organic guest molecules (GH) producing radicals ($G^\bullet$) in a secondary process:

$$H^\bullet + GH \longrightarrow H_2 + G^\bullet \quad \textbf{(3)}$$

$$OH^\bullet + GH \longrightarrow H_2O + G^\bullet \quad \textbf{(4)}$$

Neither of the two cyclic tetrahydrofuranyl radicals,[23,35] expected to form through an analogous $H^\bullet$ abstraction from THF are detected in any of our ESR spectra at 77 K. The conspicuous absence of these cyclic radicals along with the strong evidence of C-C or C-O bond cleavage constitutes a striking divergence of the induced 2PC from all prior accounts in clathrate hydrates.

The other major product detected in the ESR spectrum gives rise to a broad singlet (Fig. 4). The simplicity of this signal makes it somewhat challenging to assign but the two most plausible candidates are an acyl radical[56–58] and a trapped electron (e_t^-). Both these species have similar g-factors (~2.001) both produce a featureless singlet due to unresolved HFC. There is precedent that protons split in reaction (2) can be stabilized by ionic[31,59] and nonionic guest molecules with high proton affinities such as tert-butylamine (tBA),[28,30] enabling the detection of e_t^- in clathrate hydrates by steady-state ESR. But even in these examples, the leftover $OH^\bullet$ abstract a H atoms from the guests per reaction (4). We also noticed that this signal photobleaches when exposed to the 532 nm Raman pump laser following UV irradiation (Figs. S16-18)—an effect seen in both acyl radicals and e_t^-. The ambiguity of this assignment is largely rectified by isotopic labelling. Deuteration of water results in only a modest ~11% reduction of the singlet linewidth whereas deuteration of THF results in a ~42% reduction (Table S4). This is strong evidence in favor of the acyl radical because its measured linewidth will be broadened chiefly by unresolved HFC to intramolecular protons. Conversely, since the preferred trapping site for an electron in clathrate hydrates is likely to involve tetrahedral coordination by four water molecules at a nodal defect in the host lattice,[60] an ESR singlet corresponding to e_t^- should instead experience this significant linewidth contraction in D_2O

This journal is © The Royal Society of Chemistry 2023

Please do not adjust margins

hydrates. We conclude that the most likely identity of this signal is an acyl radical:

$$\mathrm{THF} \xrightarrow{2\times265\ \mathrm{nm}} \mathrm{R^{\bullet}C{=}O} + \mathrm{R'} \quad (5)$$

Even if we do not observe e_t^- by steady-state ESR, it may be relevant at timescales not probed in this work; we will discuss the likelihood of this in Section 2.3.

The remaining two organic radical components (Fig. 4) were much more easily identified as the three-carbon allyl radical,

$$\mathrm{THF} \xrightarrow{2\times265\ \mathrm{nm}} \mathrm{^{\bullet}CH_2CH{=}CH_2} + \mathrm{R'} \quad (6)$$

and the one-carbon methyl radical,

$$\mathrm{THF} \xrightarrow{2\times265\ \mathrm{nm}} \mathrm{^{\bullet}CH_3} + \mathrm{R'} \quad (7)$$

These radical structures indicate extensive fragmentation of the THF molecule following 2PA, consistent with a direct photolysis mechanism. We find excellent agreement between the measured and computed ESR parameters for each of our radical structural assignments (Tables S3-S6).

The characteristic signatures of atomic hydrogen (Fig. 3a & 3e) and deuterium (Fig. 3b & 3d) can be observed at both the low- and high-field ranges. While the presence of D• in samples containing either D_2O or d8-THF might initially suggest that both the host and guest are sources of these radicals, this may not be the case. Protons generated from the water framework in reaction (2) followed by exchange with guest molecules has been proposed to occur in some studies on *γ*-irradiated hydrates,[16,29] but in our system isotopic labelling provides no evidence for the incorporation of host nuclei into the enclathrated radicals. Furthermore, we detect no hydroxyl radicals (OH•) produced in our UV irradiated hydrate samples in contrast to pure water ice (Fig. S11) and *γ*-irradiated CO_2[26] and Xe[61] hydrates. A common trait of all these systems is a lack the excess of guest-bound hydrogen needed to re-form water. While the absence of OH• is expected for hydrate systems that exhibit H• abstraction reactions (3) and (4),[19–25,28] the radical formation mechanisms in our system strongly deviate from

Figure 4: ESR basis analysis for irradiated D_2O/THF clathrate hydrate at 77 K. **(a)** Measured spectrum (orange) and residual to the best fit (red). **(b)** Simulated component spectra of 1-alkyl, acyl, methyl, allyl, and atomic radicals extracted from the best-fit. Molecular structures for each species are shown in the margins with spin-density isosurfaces drawn (positive: yellow, negative: cyan). The explicit structure of the R-groups on the 1-alkyl and acyl radicals cannot be determined from ESR spectra alone. The presence of a Cu(II) internal standard is responsible for the sloped baseline at higher g-factors (see Fig. S15a for the full spectral range).

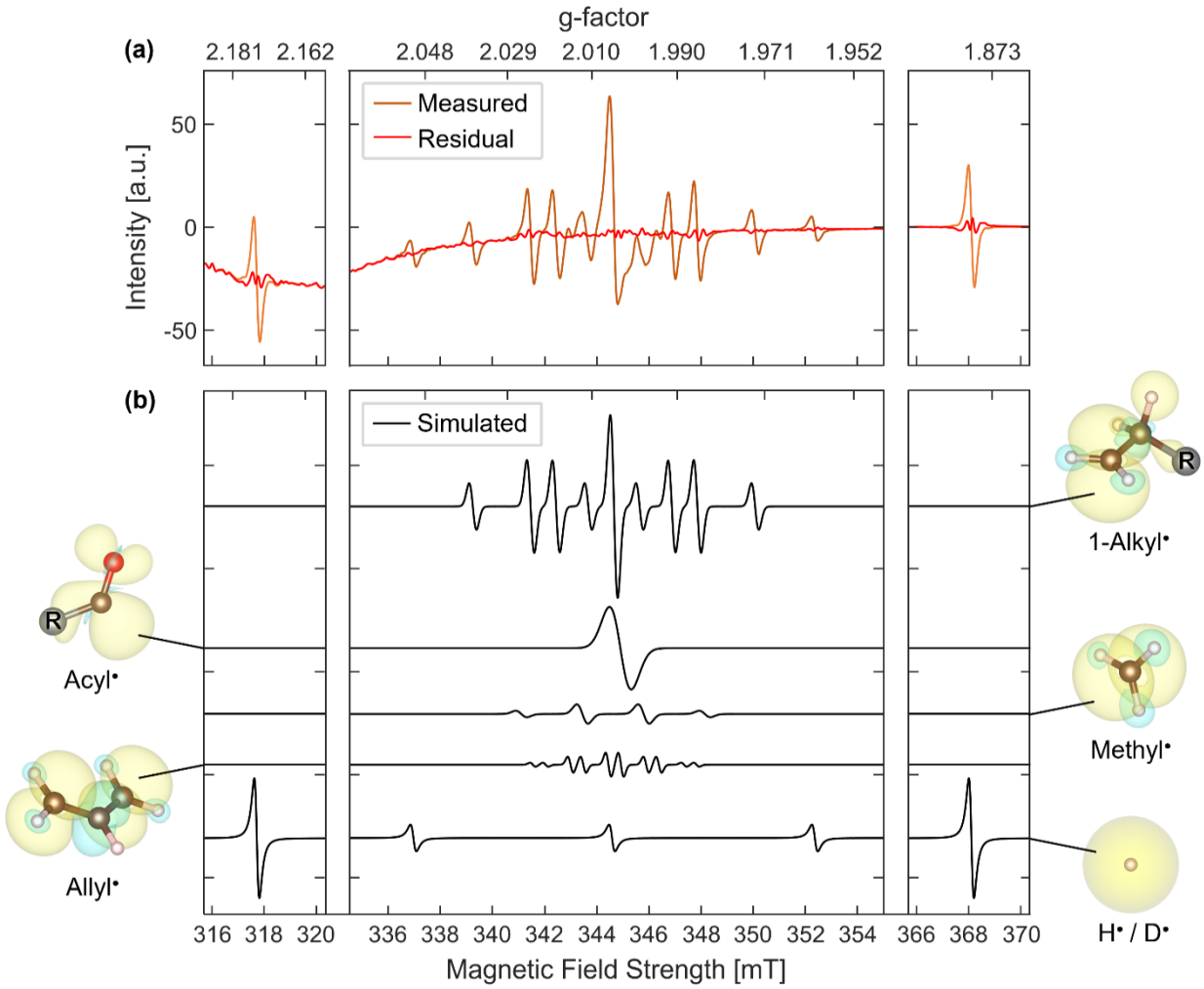

Please do not adjust margins

this motif. Conversely, we do weakly detect H• in pure glassy THF under the same irradiation conditions (Fig. S11) which is consistent with previous reports of H atom loss during VUV photolysis of THF in its pure condensed phases.[62,63] It is plausible that H•/D• fragments originating from the photolysis of the organic guests possess sufficient kinetic energy to undergo exchange with the host water[64] to explain the concurrence of both isotopes in Figure 3. Both atomic radicals are stable indefinitely at 77 K, remaining trapped at some well-defined site within the hydrate structure (perhaps within empty 5^{12} cages[65]) as evidenced by a super-hyperfine interaction (Fig. 3). Given the multiplicity of this additional splitting, and the fact that its magnitude is only large enough to be resolved in undeuterated host matrices, it might be attributed to a pair of protons of a nearby water molecule. The atomic radicals quickly decay when our samples are annealed above ~120 K, consistent with other reports.[24,26,29,38] Only at these elevated temperatures does the thermally activated diffusion of H•/D• between cages[59,60] enable reaction (3) with in-tact THF molecules to form the cyclic THF-2-yl radicals which we only detect after annealing (Fig. S12, Table S7). Alternatively, these mobile atomic radicals can terminate with organic parent fragments or each other to yield ESR silent products. Regardless of the precise origins of the atomic radicals, they are unlikely to play any role in the formation of organic radicals observed at 77 K.

2.3 The Potential Role of Trapped Electrons

Based on our estimate of $1\delta_{THF}/17\delta_{H2O}$ in Section 2.1, some ionization of water is likely to occur in our system under UV irradiation, analogous to reaction (2). The ionization threshold of water has an early onset in the condensed phase,[51,52,67–69] beginning at energies as low as ~8 eV in amorphous ice at 77 K.[70,71] Existing H-bond defects in the crystal lattice can serve as trapping sites[60] which may prolong recombination with protons. Likewise, the combined energy of two pump photons (9.36 eV) happens to fall just below the adiabatic ionization threshold of gas-phase THF (9.42 eV).[72] While we find no convincing evidence of the THF radical cation[73] or e_t^- by steady-state ESR, we cannot entirely rule them out as important short-lived intermediates without the information provided by a time-resolved study. After all, solvated electrons (e_{aq}^-) are well known to exhibit a wide array of reactivity with organic compounds in solution[74,75] so one might naturally suspect that they are responsible for the observed fragmentation of THF. In cryogenic clathrate hydrates, the low mobility of water[76] does not allow for electrons or any related anion radical intermediate to be properly solvated. Transient melting due to absorption of the pump laser might allow for solvation to occur on short timescales, however, the local temperature jump would greatly increase the energetics of atomic radicals. Since we detect an accumulation of H•/D• during irradiation and do not measure cyclic radicals at 77 K, we can place a hard upper limit on the rate of photon energy absorbed by the sample such that it cannot produce a local temperature jump higher than 120 – 77 = 43 K. Still, polaronic e_t^- has many similarities with e_{aq}^- which might facilitate a reactions with guest molecules.[77] Indeed, electron transfer to N_2O has previously been demonstrated in tBA/N_2O mixed hydrates[30,78] although in other cases e_t^- are stabilized on long timescales and do not seem to spontaneously react with guests.[28,31,59] N_2O[79] is much more readily reduced than THF[80] which itself is a popular choice of solvent for electrochemical reductions because of its wide potential window,[81] as well as in reductions with lithium metal and solvated electrons.[82] Reactive scattering studies investigating the effects of low energy electrons on structural subunits of DNA as well as THF show an onset of fragmentation beginning at ~5 eV.[75,83] However photoelectrons liberated from ice by two-photon excitation at 265 nm would not possess energies higher than ~1.4 eV[69,70] rendering THF fragmentation unlikely since its weakest bond (C-O) has a dissociation energy is ~3.6 eV.[84] As mentioned earlier, all comparable clathrate studies *including* those in THF hydrates,[23,35] employing *γ*-rays or protons with energies in excess of 1 MeV display distinct radical spectra from those we observe. We posit that these higher energy irradiation sources are *more* likely to induce electron chemistry than two-photon threshold ionization due to increased recombinational escape probability,[68,85] additional electron sources from Auger emission following core-level ionization,[86] and the possibility of electron-impact ionization.[87,88] Taken all together, we do not find sufficient evidence or precedent for the observed fragmentation of THF in clathrate hydrates to be adequately explained in terms of reactions involving trapped electrons.

2.4 Hypothesized Nonlinear Photolysis Scheme

The diversity of the observed photoproducts hints at the existence of multiple decomposition channels with similarities to those put forth by Lee *et al* to describe their molecular beam experiments.[45] Given the distribution of radicals stabilized in our hydrate samples after UV irradiation, we can only offer a hypothesis regarding the fast dynamics that unfolded immediately after two-photon excitation. Our hypothesized photolysis scheme is presented in Figure 5 and is consistent with the evidence provided. Following 2PA to a nested Rydberg manifold, gas phase THF is thought to undergo rapid interconversion to high vibrational levels of the ground electronic state, which leading to the rupture of a C-O bond.[89] For enclathrated THF, confinement of these Rydberg orbitals by neighbouring molecules[90,91] might result in a blue-shift of the associated excited states as seen in the VUV absorption spectra of water in its condensed phases (Fig. 1a).[92] Since no such absorption spectrum has been measured for THF in clathrate hydrates, we cannot specify exactly which excited state we are accessing, but as demonstrated by Röder *et. Al.*, the dynamics that follow are largely independent of the exact nature of the excited states.[89] From our estimates of the total delivered photon flux and quantitative product yields reported in Table S8, we estimate the quantum efficiency for the irradiation of the hydrate to be < 0.1%. This low absorption efficiency reflects an effective laser intensity experienced by the strongly scattering hydrate sample (Fig. S9b) that is well below the threshold for $\chi^{(>3)}$ nonlinearity and 3-photon

 This journal is © The Royal Society of Chemistry 2023

Please do not adjust margins

ionization. We can then suppose that the first step of the reaction sequence is in accord with the gas phase studies of Röder *et al.*[89] This first reaction step yields the 1,5-diradical,

$$\{\mathrm{THF}\} \xrightarrow{2 \times 265\ \mathrm{nm}} \{^{\bullet}\mathrm{CH_2CH_2CH_2CH_2O}^{\bullet}\} \quad \textbf{(8)}$$

where the curly brackets denote a clathrate cage enclosing the molecule. This diradical may re-cyclize[62,63] or undergo rapid thermal decomposition[93,94] to give the observed fragments. The extent of this fragmentation prior to quenching is partially determined by the efficiency of vibrational coupling of the excited guest to the surrounding host lattice.[95] It has been suggested elsewhere that β-elimination from the nascent 1,5-diradical may result in two energetically plausible hydrogen-loss channels.[96] The first involves the loss of H$^{\bullet}$ from the 2-position and the formation of a C=O double bond:

$$\{^{\bullet}\mathrm{CH_2CH_2CH_2CH_2O}^{\bullet}\} \longrightarrow \{^{\bullet}\mathrm{CH_2CH_2CH_2CH{=}O}\} + \{\mathrm{H}^{\bullet}\} \quad \textbf{(9)}$$

Following reaction (9), the observed terminal alkyl radical might result from C-C bond cleavage and successful diffusion of translationally hot CO from its original cage[97–102] to yield an isolated n-propyl radical:

$$\{^{\bullet}\mathrm{CH_2CH_2CH_2CH{=}O}\} \longrightarrow \{^{\bullet}\mathrm{CH_2CH_2CH_3}\} + \{\mathrm{CO}\} \quad \textbf{(10)}$$

However, if CO remains trapped and fails to diffuse from its original cage, it may spontaneously rearrange with the n-propyl radical to form the butanoyl radical (Table S4), which is a likely candidate for the acyl radical:

$$\{^{\bullet}\mathrm{CH_2CH_2CH_3} + \mathrm{CO}\} \longrightarrow \{\mathrm{O{=}^{\bullet}C\text{-}CH_2CH_2CH_3}\} \quad \textbf{(11)}$$

Photobleaching of the acyl radical with visible light (Figs. S16-18) effectively reverses this process, regenerating 1-alkyl radicals and CO:[56–58]

$$\{\mathrm{O{=}^{\bullet}C\text{-}CH_2CH_2CH_3}\} \xrightarrow{532\ \mathrm{nm}} \{^{\bullet}\mathrm{CH_2CH_2CH_3}\} + \{\mathrm{CO}\} \quad \textbf{(11*)}$$

Similarly, following reaction (9), the methyl radical (Table S5) might also escape after forming through the simultaneous cleavage of two C-C bonds and H atom transfer to methylene:

$$\{^{\bullet}\mathrm{CH_2CH_2CH_2CH{=}O}\} \longrightarrow \{\mathrm{CO} + \mathrm{CH_2{=}CH_2}\} + \{^{\bullet}\mathrm{CH_3}\} \quad \textbf{(12)}$$

If this highly reactive species remains confined with its sister fragments, n-propyl and butanoyl radicals will form:

$$\{\mathrm{CH_2{=}CH_2} + {}^{\bullet}\mathrm{CH_3}\} + \{\mathrm{CO}\} \longrightarrow \{^{\bullet}\mathrm{CH_2CH_2CH_3}\} + \{\mathrm{CO}\} \quad \textbf{(13)}$$

$$\{\mathrm{CO} + \mathrm{CH_2{=}CH_2} + {}^{\bullet}\mathrm{CH_3}\} \longrightarrow \{\mathrm{O{=}^{\bullet}C\text{-}CH_2CH_2CH_3}\} \quad \textbf{(14)}$$

The second hydrogen-loss channel[96] from the 1,5-diradical involves β-elimination of H$^{\bullet}$ from the 4-position and the formation of a C=C double bond:

$$\{^{\bullet}\mathrm{CH_2CH_2CH_2CH_2O}^{\bullet}\} \longrightarrow \{\mathrm{CH_2{=}CHCH_2CH_2O}^{\bullet}\} + \{\mathrm{H}^{\bullet}\} \quad \textbf{(15)}$$

A subsequent C-C bond cleavage from the resulting oxyl radical yields an allyl radical (Table S6) alongside formaldehyde:

$$\{\mathrm{CH_2{=}CHCH_2CH_2O}^{\bullet}\} \longrightarrow \{^{\bullet}\mathrm{CH_2CH{=}CH_2} + \mathrm{H_2C{=}O}\} \quad \textbf{(16)}$$

Due to its size, formaldehyde may not easily migrate out of its original cage. However, unlike with reaction (11), a stable structure was successfully calculated for a doubly occupied cage containing formaldehyde and the allyl radical. It is plausible that resonance stabilization of the allyl radical's unpaired electron prevents a spontaneous reverse reaction with

Figure 5: Hypothesized scheme for the two-photon photolysis of enclathrated THF (cages not drawn to scale). H-bonds lying along cage edges are denoted with grey lines with implicit water molecules at the vertices. Following two-photon UV excitation, homolytic C-O bond cleavage and ultrafast ring-opening (8), the thermal decomposition proceeding on the electronic ground state is quenched by the stabilizing hydrate network to yield radical intermediates observable by steady-state ESR spectroscopy at 77 K (highlighted in pink). Dashed arrows indicate recombination of fragments within clathrate cages. Green arrows indicate the photobleaching of the acyl radical (11*) by visible light (see Figs. S16-18). The thickness of the arrows is suggestive of the relative branching ratios. Spin-density isosurfaces are drawn for each radical (positive: yellow, negative: cyan). Arrow labels reference reactions described in this section of the text. Optimized structures within clathrate cages and their computed relative energies are presented in Figure S19.

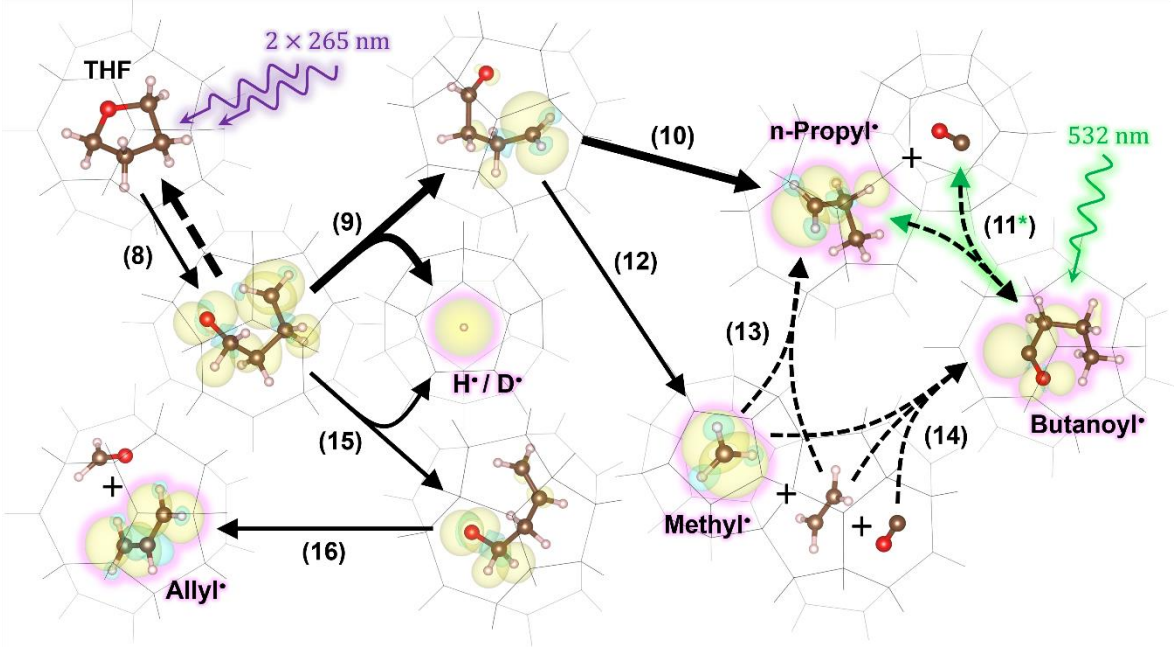

Please do not adjust margins

formaldehyde:

$$[^{\bullet}CH_2CH{=}CH_2 \longleftrightarrow CH_2{=}CHCH_2^{\bullet}] \quad \textbf{(17)}$$

It is important to note that none of the diamagnetic products proposed in the above scheme (CO, ethylene, and formaldehyde) could be observed directly by NMR or Raman spectroscopy. Likewise, no products resulting from the decay of the ESR active radicals could be detected after thawing the irradiated hydrate samples at ambient temperature.

3 Conclusions and Outlook

Spectroscopists already routinely employ sequences of ultrafast excitation pulses to investigate the relaxation dynamics of high-lying electronic states of molecules, however the complexity of these experiments and the high sensitivity of ESR spectroscopy to radical species makes a degenerate 2PA scheme an attractive alternative. Furthermore, the trapping of reaction products in clathrate hydrates enable the detection of molecules that are otherwise short lived in the condensed phase. In this work, we demonstrated that ultrafast pulsed lasers, which are commercially widely available, can be a powerful tool for condensed phase 2PC. When assessing the selectivity of 2PA in THF hydrates, we conclude that THF absorbs the 265 nm radiation at nearly the same rate as water despite having a 17-fold disparity in concentration. ESR measurements following irradiation at 77 K clearly reveal the presence of several organic radical fragments originating exclusively from the photolysis of THF rather than as a consequence of water splitting. While we cannot definitively rule out any potential involvement of trapped electrons in the fast dynamics, we conclude that their role is most likely that of transient spectators.

THF is often used as a simple molecular analog to the ribose backbone of DNA.[75,83,86–88,103–107] In our system, the network of the hydrate approximates its aqueous environment which strongly influences the outcomes of related radiation induced processes.[108] Astrochemical insights can also be gleaned since extraterrestrial clathrate hydrates are often implicated in the irradiation chemistry of interstellar and planetary ices.[109–116] This work showcases and extends the potential of clathrate hydrates as a useful and interesting condensed phase reaction medium through the novel use of 2PA and its incitement of a distinct radical formation mechanism.

In principle 2PA could enable selective excited-state photochemistry of solute molecules within a variety of other condensed phase systems. Molecular 2PA cross-sections can be tuned by combining photons with different polarizations and energies in experiments involving multiple laser beams,[9] presenting further opportunities for additional state and solute selectivity afforded by 2PA beyond those explored here. The choice of this tailored excitation might be informed by a computation of the relative energies and cross-sections for excited states accessible under 2PA selection rules for a given photon pairing and molecular system.[117,118] The simultaneous absorption of three or more photons (N-photon absorption) to access even higher-lying states, could further extend the capabilities of existing light sources while maintaining the material transparency and dispersive properties enjoyed at longer wavelengths.

4 Methods

4.1 Laser Specifications

The 265 nm 3rd harmonic of Ti:Sapphire laser light was used as an irradiation source (SI.1a) and its intensity profile $I_z(r,t)$ was characterized along the beam axis z, both radially r, and in time t. The maximum pulse energy E_0 incident onto the sample was ~2 μJ and the repetition rate was 5 kHz. The full-width $1/e^2$ pulse duration $\tau_{pulse} = 4\tau$ (assuming Gaussian profile in time) was determined to be 504 ± 78 fs from an intensity autocorrelation (SI.1b) utilizing 2PA in liquid water.[119] The focused beam was spatially profiled (SI.1c) to give an M^2 of 5.63, though Gaussian fits along the transverse axes are well-behaved (Fig. S4b). We therefore consider for our beam's spatial profile acceptably close to a Gaussian with an incident peak intensity given by:

$$I_0(0,0) = \frac{\sqrt{2}\,E_0}{\pi^{3/2} w_0^2 \tau} \quad \textbf{Eqn.1}$$

For all experiments performed herein, τ, and w_0 remain fixed while $I_0(0,0)$ is modulated by varying E_0 (this is achieved through the rotation of an up-stream waveplate).

4.2 Irradiation of Liquid Samples

Transmittance measurements were performed using a f = 500 mm lens to produce a focus with a $1/e^2$ waist radius of 142 ± 2 μm (Rayleigh range of 5.7 ± 0.6 cm) and assumed to remain roughly constant through the 1 cm samples. Equation 1 gives a maximum incident peak intensity of ~20 GW/cm^2. A pair of GaP photodiodes (SM05PD7A) were placed before and after sample calibrated with a power meter such that the time-integrated voltage could converted to incident and transmitted pulse energy (Fig. S2). The transmitted energy of a pulse with a Gaussian intensity profile in space and time and a constant beam diameter through a sample of length L undergoing 2PA is given by:[49]

$$E_L = \frac{\pi w_0^2}{2\beta L} \int_{-\infty}^{+\infty} \ln\left[1 + \beta L I_0(0,0) e^{-t^2/2\tau^2}\right] dt \quad \textbf{Eqn.2}$$

This expression was evaluated numerically and divided by the incident pulse energy to obtain the transmittance:

$$T = E_L/E_0 \quad \textbf{Eqn.3}$$

The measured incident and transmitted pulse energies were corrected for Fresnel reflection at each interface at normal incidence as well as absorption by the 1 mm quartz cuvette windows. The 2PA coefficients β were determined by fitting the corrected transmittance measurements to the theory. 2PA cross-sections were then calculated using the ground state

This journal is © The Royal Society of Chemistry 2023

Please do not adjust margins

number density N_g of the absorber and the photon energy $\hbar\omega$:

$$\delta = \beta\hbar\omega/N_g \quad \textbf{Eqn.4}$$

The best fit values of β and δ are reported in Table 1.

4.3 Preparation and Irradiation of Cryogenic Samples

Nanopure water was sparged with a stream of dry N_2 gas for several minutes to drive out any dissolved oxygen, then placed in a sonicator for ~1 hour to degas. THF (inhibitor-free) was purchased from Fisher Scientific and sparged for 20 min with dry Argon and dried using a commercial two-column solvent purification system (LC Technologies). It was then further dried by storing over 3 Å molecular sieves for at least 48 hours prior to use. A sealed ampule of d8-THF (≥ 99.5 atom % D) was purchased from Sigma-Adlrich.

Three stock solutions consisting of THF:H_2O, THF:D_2O, and d8-THF:H_2O in 1:17 molar ratios were prepared in glass walled, PTFE capped bottles. Solutions stored in a refrigerator just above the freezing point of water (1 °C for H_2O and 5 °C for D_2O) to promote hydrate growth but prevent freezing (Fig. S6). After several hours of refrigeration, bottles were repeatedly dipped in liquid nitrogen for short intervals to encourage nucleation, and then placed back into the refrigerator. Within ~1 hour, the stock solutions had fully solidified into a hydrate. Small pieces of the crystallized stock solution were dropped in a shallow bath of liquid nitrogen, crushed into fine gains (~1 mm in diameter), and packed into ESR tubes, which were then gently submerged into a filled Wilmad-LabGlass ESR cold finger liquid nitrogen Dewar (WG-816-D-Q). The samples presented to the laser took on a snow-like appearance (Fig. S15b). To compensate for the rapid drop in laser intensity due to scattering in the sample, the pump light was focused tightly using a f = 40 mm lens. With these focal conditions, satisfactory signal-to-noise was obtained after 2 hours of UV irradiation. During irradiation, the sample was continuously translated vertically and rotated so that the laser traced a helical path. This is done to increase yield and prevent heating of the sample by the pump laser. An illustration of the setup as described can be found in Figure S5.

4.4 Characterization of Cryogenic Samples

For the quantitation of enclathrated radicals presented in Table S8, 34.1 ± 0.4 μmol of copper(II) sulfate pentahydrate was placed in a sealed vessel beneath the THF hydrate sample (Fig. 15b & c) and out of the path of the incident laser beam to act as an internal standard. The relative signal areas of the component spectra (Fig. 4b) and were calibrated to the standard using Equation S4, which accounts for the *g*-dependence of the ESR transition probability.[120]

Raman spectra (Figs. S7-9) were measured to assess sample structure and composition before and after irradiation. The 532 nm Raman laser was collinear with the 265 nm pump laser and the backscatter was fiber-coupled into an ARC SpectraPro-300i (details in SI.2b). From the normalized difference spectra in Figure S8, virtually no changes associated with product formation, reactant consumption, or decomposition of the hydrate structure are apparent even after 4 hours of scanning with the focused UV laser beam. This is consistent, both with our estimates of the accumulated radical concentrations (see SI.3e) lying far below the spontaneous Raman limit of detection, and with the background-free measurements of long-lived radicals by ESR.

After UV irradiation, the liquid nitrogen cold finger containing the hydrate samples were transferred to a Bruker EMX Premium-X EPR Spectrometer. The microwave cavity was tuned to an X-band frequency of ~9.67 GHz for spectra measured at 77 K, and the power used was 5 mW. Data analysis, spectral simulations, and fitting were done using the EasySpin MATLAB toolbox.[121] The simulated spin systems used to obtain best-fits to the measured spectra provided the information on atomic connectivity necessary to propose the candidate structures in the margins of Figure 4.

4.5 Electronic Structure Calculations

Optimized structures were calculated using Vienna Ab initio Simulation Package (VASP)[122–124] employing the revised Perdew-Burke-Ernzerhof (revPBE) exchange correlation functional[125,126] with the DFT-D3 dispersion correction[127] and Becke-Johnson damping function.[128] This approach has been validated in computational studies on CO_2 clathrate hydrates for its accurate treatment of non-covalent, host-guest interactions.[129] A plane-wave basis set with the projector augmented wave (PAW)[130] method was employed. The atomic coordinates for the water molecules constituting the sII hydrate framework were taken from Lenz and Ojamäe[131] with guest molecules placed into their initial positions at the centers of empty $5^{12}6^4$ cavities. During the optimizations, which ran the conjugate gradient algorithm with a minimum force cutoff of 0.005 eV/Å, all atoms of the guest molecules were relaxed while those of the 28 waters comprising the cage remained fixed. The VASPKIT add-on[132] was used to generate spin density plots from the valence charge density.

Single-point DFT calculations were performed on the optimized candidate radical structures using the Orca quantum chemistry program[133,134] to obtain hyperfine coupling constants and *g*-tensors. For this, the EPR-III basis set[135,136] was used with the gauge invariant atomic orbital (GIAO) approach[137,138] and B3LYP functional.[139–142]

Author Contributions

M. A. M. conceived of the project. M. A. M. designed the experiments. C. R. P., M. A. M. and P. C. constructed the laser system. P. C. built and configured the Raman spectrometer. M. A. M. performed the experiments. M. A. M. performed the simulations. All authors made intellectual contributions, discussed the results and commented on the manuscript.

Conflicts of interest

There are no conflicts to declare.

Acknowledgements

This project was supported, in part, by the Army Research Office, Award # W911NF-19-1-0178.

Dr. N. P. Vargo contributed scientific insights and loaned vital laboratory equipment.

We would like to thank Prof. H. Jónsson at the University of Iceland for his guidance with running electronic structure calculations, H. Garces, Facility Manager at Brown IMNI NanoTools Facility for providing ESR instrument training. We are also grateful for the parallel research contributions and expertise of fellow group members Dr. P. Chmielniak, Dr. Z. Li and Dr. M. Lyu which were invaluable to this work.

We would also like to thank Dr. B. B. Pate and Dr. K. E. Whitener at U. S. Naval Research Laboratory for their knowledge regarding solvated and trapped electrons.

All calculations were run on Brown University's high performing computing cluster, Oscar.

Notes and references

§ Stoichiometric THF hydrates imply the full occupancy of the large cages by THF and are grown from aqueous solutions with a 1:17 (8:136) molar ratio of THF and H_2O.

1 N. Thantu and P. M. Weber, *Z Phys D - Atoms, Molecules and Clusters*, 1993, **28**, 191–194.
2 M. P. Minitti, Y. Zhang, M. Rosenberg, R. Y. Brogaard, S. Deb, T. I. Sølling and P. M. Weber, *J. Phys. Chem. A*, 2012, **116**, 810–819.
3 J. C. Netto-Ferreira, V. Wintgens and J. C. Scaiano, *Tetrahedron Letters*, 1989, **30**, 6851–6854.
4 A. Ouchi, Z. Li, M. Sakuragi and T. Majima, *J. Am. Chem. Soc.*, 2003, **125**, 1104–1108.
5 J. Bendig and R. Mitzner, *Berichte der Bunsengesellschaft für physikalische Chemie*, 1994, **98**, 1004–1008.
6 C. P. Schick, S. D. Carpenter and P. M. Weber, *J. Phys. Chem. A*, 1999, **103**, 10470–10476.
7 M. Göppert-Mayer, *Annalen der Physik*, 1931, **401**, 273–294.
8 M. Göppert, *Naturwissenschaften*, 1929, **17**, 932–932.
9 C. G. Elles, C. A. Rivera, Y. Zhang, P. A. Pieniazek and S. E. Bradforth, *J. Chem. Phys.*, 2009, **130**, 084501.
10 D. Strickland and G. Mourou, *Opt. Commun*, 1985, 219–221.
11 P. Maine, D. Strickland, P. Bado, M. Pessot and G. Mourou, *IEEE Journal of Quantum Electronics*, 1988, **24**, 398–403.
12 D. Yang, S. J. Jhaveri and C. K. Ober, *MRS Bulletin*, 2005, **30**, 976–982.
13 V. Hahn, F. Mayer, M. Thiel and M. Wegener, *Optics & Photonics News, OPN*, 2019, **30**, 28–35.
14 W. Zong, R. Wu, S. Chen, J. Wu, H. Wang, Z. Zhao, G. Chen, R. Tu, D. Wu, Y. Hu, Y. Xu, Y. Wang, Z. Duan, H. Wu, Y. Zhang, J. Zhang, A. Wang, L. Chen and H. Cheng, *Nat Methods*, 2021, **18**, 46–49.
15 W. Denk and K. Svoboda, *Neuron*, 1997, **18**, 351–357.
16 Z. Zhou, J. Liu, J. Huang, T. W. Rees, Y. Wang, H. Wang, X. Li, H. Chao and P. J. Stang, *Proceedings of the National Academy of Sciences*, 2019, **116**, 20296–20302.
17 K. Takeya, K. Nango, T. Sugahara, K. Ohgaki and A. Tani, *J. Phys. Chem. B*, 2005, **109**, 21086–21088.
18 K. Takeya, A. Tani, T. Yada and M. Ikeya, *Applied Radiation and Isotopes*, 2005, **62**, 371–374.
19 K. Takeya, K. Nango, T. Sugahara, K. Ohgaki, A. Tani, H. Ito, M. Okada and T. Kasai, *Jpn. J. Appl. Phys.*, 2007, **46**, 3066–3070.
20 K. Takeya, T. Sugahara, K. Ohgaki and A. Tani, *Radiation Measurements*, 2007, **42**, 1301–1306.
21 K. Takeya, A. Tani, T. Yada, M. Ikeya and K. Ohgaki, *Jpn. J. Appl. Phys.*, 2004, **43**, 353–357.
22 K. Ohgaki, K. Nakatsuji, K. Takeya, A. Tani and T. Sugahara, *Physical Chemistry Chemical Physics*, 2008, **10**, 80–82.
23 S.-H. Yeon, J. Seol, Y. Park, D.-Y. Koh, Y. S. Kang and H. Lee, *J. Am. Chem. Soc.*, 2008, **130**, 9208–9209.
24 T. Sugahara, Y. Kobayashi, A. Tani, T. Inoue and K. Ohgaki, *J. Phys. Chem. A*, 2012, **116**, 2405–2408.
25 M. Oshima, K. Kitamura, A. Tani, T. Sugahara and K. Ohgaki, *J. Phys. Chem. B*, 2014, **118**, 13435–13439.
26 M. Oshima, A. Tani, T. Sugahara, K. Kitano and K. Ohgaki, *Phys. Chem. Chem. Phys.*, 2014, **16**, 3792.
27 M. Cha, K. Shin, M. Kwon, D.-Y. Koh, B. Sung and H. Lee, *J. Am. Chem. Soc.*, 2010, **132**, 3694–3696.
28 A. Tani, S. Koyama, Y. Urabe, K. Takato, T. Sugahara and K. Ohgaki, *J. Phys. Chem. B*, 2014, **118**, 13409–13413.
29 K. Shin, M. Cha, H. Kim, Y. Jung, Y. S. Kang and H. Lee, *Chem. Commun.*, 2011, **47**, 674–676.
30 Y.-H. Ahn, D. Lim, J. Min, J. Kim, B. Lee, J. W. Lee and K. Shin, *Chemical Engineering Journal*, 2019, **359**, 1629–1634.
31 J. Bednarek, A. Lund and S. Schlick, *J. Phys. Chem.*, 1996, **100**, 3910–3916.
32 D.-Y. Koh, H. Kang, J. Park, W. Shin and H. Lee, *J. Am. Chem. Soc.*, 2012, **134**, 5560–5562.
33 P. Goldberg, *Science*, 1963, **142**, 378–379.
34 Y. Ding, Investigation of free radicals in clathrate hydrates using electron paramagnetic resonance spectroscopy, https://summit.sfu.ca/item/34491, (accessed August 28, 2022).
35 S. Moon, S. Hong, Y. Lee, J. S. Lee, Y.-H. Ahn and Y. Park, *J. Phys. Chem. C*, 2021, **125**, 1767–1773.
36 M. Mozafari, L. Chandrasena, I. McKenzie, K. Samedov and P. W. Percival, *Radiation Physics and Chemistry*, 2020, **168**, 108532.
37 M. Mozafari, J.-C. Brodovitch, L. Chandrasena and P. W. Percival, *J. Phys. Chem. A*, 2016, **120**, 8521–8528.
38 M. Mozafari, L. Chandrasena, I. McKenzie, K. Samedov and P. W. Percival, *Can. J. Chem.*, 2018, **96**, 217–225.
39 P. W. Percival, M. Mozafari, J.-C. Brodovitch and L. Chandrasena, *J. Phys. Chem. A*, 2014, **118**, 1162–1167.
40 M. Ceppatelli, R. Bini and V. Schettino, *Phys. Chem. Chem. Phys.*, 2011, **13**, 1264–1275.
41 R. Larsen, C. A. Knight and E. D. Sloan, *Fluid Phase Equilibria*, 1998, **150–151**, 353–360.
42 K. A. Udachin, C. I. Ratcliffe and J. A. Ripmeester, *Journal of Supramolecular Chemistry*, 2002, **2**, 405–408.
43 T. Makino, T. Sugahara and K. Ohgaki, *J. Chem. Eng. Data*, 2005, **50**, 2058–2060.
44 S. Sengupta, J. Guo, K. C. Janda and R. W. Martin, *J. Phys. Chem. B*, 2015, **119**, 15485–15492.
45 S.-H. Lee, *Phys. Chem. Chem. Phys.*, 2010, **12**, 2655.
46 G. D. Kerr, R. N. Hamm, M. W. Williams, R. D. Birkhoff and L. R. Painter, *Phys. Rev. A*, 1972, **5**, 2523–2527.
47 M. Seki, K. Kobayashi and J. Nakahara, *J. Phys. Soc. Jpn.*, 1981, **50**, 2643–2648.
48 A. Giuliani, P. Limão-Vieira, D. Duflot, A. R. Milosavljevic, B. P. Marinkovic, S. V. Hoffmann, N. Mason, J. Delwiche and M.-J. Hubin-Franskin, *Eur. Phys. J. D*, 2009, **51**, 97–108.
49 M. Rumi and J. W. Perry, *Adv. Opt. Photon.*, 2010, **2**, 451.
50 A. Dragonmir, J. G. McInerney and D. N. Nikogosyan, *Appl. Opt., AO*, 2002, **41**, 4365–4376.
51 C. L. Thomsen, D. Madsen, S. R. Keiding, J. Thøgersen and O. Christiansen, *The Journal of Chemical Physics*, 1999, **110**, 3453–3462.
52 D. N. Nikogosyan, A. A. Oraevsky and V. I. Rupasov, *Chemical Physics*, 1983, **77**, 131–143.

 This journal is © The Royal Society of Chemistry 2023

Please do not adjust margins

53 P. Liu, W. L. Smith, H. Lotem, J. H. Bechtel, N. Bloembergen and R. S. Adhav, *Phys. Rev. B*, 1978, **17**, 4620–4632.
54 S. K. Garg, D. W. Davidson and J. A. Ripmeester, *Journal of Magnetic Resonance (1969)*, 1974, **15**, 295–309.
55 C. Gutt, W. Press, A. Hüller, J. S. Tse and H. Casalta, *J. Chem. Phys.*, 2001, **114**, 4160–4170.
56 A. G. Davies, R. Sutcliffe, L. Wc and H. Oaj, *J. Chem. Soc., Perkin Trans. 2.,* 1980, **5**, 819–824.
57 H. S. Judeikis and S. Siegel, *The Journal of Chemical Physics*, 2004, **43**, 3625–3638.
58 S. Noda, K. Fueki and Z. Kuri, *The Journal of Chemical Physics*, 1968, **49**, 3287–3292.
59 J. Bednarek, R. Erickson, A. Lund and S. Schlick, *J. Am. Chem. Soc.*, 1991, **113**, 8990–8991.
60 H. Huang, L. Xue, G. Lu, S. Cheng and Y. Bu, *The Journal of Chemical Physics*, 2023, **158**, 114504.
61 K. Takeya, A. Tani, T. Sugahara and K. Ohgaki, *Physics and Chemistry of Ice 2010*, 2011, 267–271.
62 A. A. Scala and W. J. Rourke, *Journal of Photochemistry*, 1987, **37**, 281–292.
63 N. Klzilkilic and H.-P. Schuchmann, 1980, **58**, 8.
64 B. Fu and D. H. Zhang, *The Journal of Chemical Physics*, 2012, **136**, 194301.
65 L. Liu, S. Mao, Q. Li, X. Wang, M. Yang and L. Li, *RSC Adv.*, 2017, **7**, 14537–14543.
66 S. Alavi and J. A. Ripmeester, *Chemical Physics Letters*, 2009, **479**, 234–237.
67 D. M. Bartels and R. A. Crowell, *J. Phys. Chem. A*, 2000, **104**, 3349–3355.
68 C. G. Elles, A. E. Jailaubekov, R. A. Crowell and S. E. Bradforth, *The Journal of Chemical Physics*, 2006, **125**, 044515.
69 V. Poterya, M. Fárník, M. Ončák and P. Slavíček, *Phys. Chem. Chem. Phys.*, 2008, **10**, 4835–4842.
70 B. Baron and F. Williams, *The Journal of Chemical Physics*, 2008, **64**, 3896–3897.
71 R. Smoluchowski, *International Astronomical Union Colloquium*, 1977, **39**, 47–49.
72 S. M. Park, Y. R. Lee, D. W. Kang, H. L. Kim and C. H. Kwon, *Phys. Chem. Chem. Phys.*, 2017, **19**, 30362–30369.
73 H. Kubodera, T. Shida and K. Shimokoshi, *J. Phys. Chem.*, 1981, **85**, 2583–2586.
74 R. Daily and D. Minakata, *Environmental Science: Water Research & Technology*, 2022, **8**, 543–574.
75 B. Boudaïffa, P. Cloutier, D. Hunting, M. A. Huels and L. Sanche, *Science*, 2000, **287**, 1658–1660.
76 S. S. N. Murthy, *Phase Transitions*, 2002, **75**, 487–506.
77 I. A. Taub and K. Eiben, *The Journal of Chemical Physics*, 2003, **49**, 2499–2513.
78 Z. P. Zagórski, *Chemical Physics Letters*, 1985, **115**, 507–510.
79 R. Deeba, S. Chardon-Noblat and C. Costentin, *Chemical Science*, 2021, **12**, 12726–12732.
80 M. Lyu, Z. Li, M. van den Bossche, H. Jónsson and C. Rose-Petruck, *Chemical Physics*, 2023, **568**, 111839.
81 R. Baron, N. M. Kershaw, T. J. Donohoe and R. G. Compton, *Journal of Physical Organic Chemistry*, 2009, **22**, 1136–1141.
82 A. A. H. Kadhum and G. A. Salmon, *J. Chem. Soc., Faraday Trans. 1*, 1986, **82**, 2521–2530.
83 M. A. Huels, L. Parenteau and L. Sanche, *J. Phys. Chem. B*, 2004, **108**, 16303–16312.
84 J. H. S. Green, *Q. Rev. Chem. Soc.*, 1961, **15**, 125–152.
85 R. A. Crowell and D. M. Bartels, *J. Phys. Chem.*, 1996, **100**, 17940–17949.
86 W. Wolff, B. Rudek, L. A. da Silva, G. Hilgers, E. C. Montenegro and M. G. P. Homem, *J. Chem. Phys.*, 2019, **151**, 064304.
87 M. Neustetter, M. Mahmoodi-Darian and S. Denifl, *J. Am. Soc. Mass Spectrom.*, 2017, **28**, 866–872.
88 E. Wang, X. Ren, W. Baek, H. Rabus, T. Pfeifer and A. Dorn, *Nat Commun*, 2020, **11**, 2194.
89 A. Röder, A. B. Skov, A. E. Boguslavskiy, R. Lausten and A. Stolow, *Phys. Chem. Chem. Phys.*, 2020, **22**, 26241–26254.
90 M. Chergui and N. Schwentner, *Chemical Physics Letters*, 1994, **219**, 237–242.
91 P. H. Hahn, W. G. Schmidt, K. Seino, M. Preuss, F. Bechstedt and J. Bernholc, *Phys. Rev. Lett.*, 2005, **94**, 037404.
92 T. W. Marin, I. Janik, D. M. Bartels and D. M. Chipman, *Nature Communications*, 2017, **8**, 15435.
93 J. Kramer, *J. Phys. Chem.*, 1982, **86**, 26–35.
94 C. H. Klute and W. D. Walters, *J. Am. Chem. Soc.*, 1946, **68**, 506–511.
95 M. Kato, S. Matsumoto, A. Takashima, Y. Fujii, Y. Takasu and I. Nishio, *Vibrational Spectroscopy*, 2016, **85**, 11–15.
96 A. A. Scala, E. W.-G. Diau, Z. H. Kim and A. H. Zewail, *The Journal of Chemical Physics*, 1998, **108**, 7933–7936.
97 S. Alavi and J. A. Ripmeester, *Angewandte Chemie International Edition*, 2007, **46**, 6102–6105.
98 D.-Y. Koh, H. Kang and H. Lee, *Korean J. Chem. Eng.*, 2015, **32**, 350–353.
99 I. L. Moudrakovski, K. A. Udachin, S. Alavi, C. I. Ratcliffe and J. A. Ripmeester, *J. Chem. Phys.*, 2015, **142**, 074705.
100 H. Lo, M.-T. Lee and S.-T. Lin, *J. Phys. Chem. C*, 2017, **121**, 8280–8289.
101 B. Peters, N. E. R. Zimmermann, G. T. Beckham, J. W. Tester and B. L. Trout, *J. Am. Chem. Soc.*, 2008, **130**, 17342–17350.
102 Á. Vidal-Vidal, M. Pérez-Rodríguez and M. M. Piñeiro, *RSC Adv.*, 2016, **6**, 1966–1972.
103 A. Zecca, C. Perazzolli and M. J. Brunger, *J. Phys. B: At. Mol. Opt. Phys.*, 2005, **38**, 2079.
104 M. Allan, *J. Phys. B: At. Mol. Opt. Phys.*, 2007, **40**, 3531.
105 X. Ren, T. Pflüger, M. Weyland, W. Y. Baek, H. Rabus, J. Ullrich and A. Dorn, *The Journal of Chemical Physics*, 2014, **141**, 134314.
106 E. Erdmann, M.-C. Bacchus-Montabonel and M. Łabuda, *Phys. Chem. Chem. Phys.*, 2017, **19**, 19722–19732.
107 X. Ren, E. Wang, A. D. Skitnevskaya, A. B. Trofimov, K. Gokhberg and A. Dorn, *Nature Phys*, 2018, **14**, 1062–1066.
108 S. J. Harris, D. Murdock, Y. Zhang, T. A. A. Oliver, M. P. Grubb, A. J. Orr-Ewing, G. M. Greetham, I. P. Clark, M. Towrie, S. E. Bradforth and M. N. R. Ashfold, *Phys. Chem. Chem. Phys.*, 2013, **15**, 6567.
109 K. P. Hand, C. F. Chyba, R. W. Carlson and J. F. Cooper, *Astrobiology*, 2006, **6**, 463–482.
110 O. Prieto-Ballesteros, J. S. Kargel, M. Fernández-Sampedro, F. Selsis, E. S. Martínez and D. L. Hogenboom, *Icarus*, 2005, **177**, 491–505.
111 S. W. Kieffer, X. Lu, C. M. Bethke, J. R. Spencer, S. Marshak and A. Navrotsky, *Science*, 2006, **314**, 1764–1766.
112 S. L. Miller and W. D. Smythe, *Science*, 1970, **170**, 531–533.
113 N. J. Mason, A. Dawes, P. D. Holtom, R. J. Mukerji, M. P. Davis, B. Sivaraman, R. I. Kaiser, S. V. Hoffmann and D. A. Shaw, *Faraday Discuss.*, 2006, **133**, 311–329.
114 S. Kamata, F. Nimmo, Y. Sekine, K. Kuramoto, N. Noguchi, J. Kimura and A. Tani, *Nat. Geosci.*, 2019, **12**, 407–410.
115 D. Blake, L. Allamandola, S. Sandford, D. Hudgins and F. Freund, *Science*, 1991, **254**, 548–551.
116 J. Ghosh, R. R. J. Methikkalam, R. G. Bhuin, G. Ragupathy, N. Choudhary, R. Kumar and T. Pradeep, *Proceedings of the National Academy of Sciences*, 2019, **116**, 1526–1531.
117 P. Sałek, O. Vahtras, J. Guo, Y. Luo, T. Helgaker and H. Ågren, *Chemical Physics Letters*, 2003, **374**, 446–452.
118 M. T. P. Beerepoot, D. H. Friese, N. H. List, J. Kongsted and K. Ruud, *Phys. Chem. Chem. Phys.*, 2015, **17**, 19306–19314.

119 E. Z. Chong, T. F. Watson and F. Festy, *Appl. Phys. Lett.*, 2014, **105**, 062111.
120 Dieter. Siebert, Juergen. Dahlem and Vitaly. Nagy, *Anal. Chem.*, 1994, **66**, 2640–2646.
121 S. Stoll and A. Schweiger, *Journal of Magnetic Resonance*, 2006, **178**, 42–55.
122 G. Kresse and J. Hafner, *Phys. Rev. B*, 1993, **47**, 558–561.
123 G. Kresse and J. Furthmüller, *Computational Materials Science*, 1996, **6**, 15–50.
124 G. Kresse and J. Furthmüller, *Phys. Rev. B*, 1996, **54**, 11169–11186.
125 J. P. Perdew, K. Burke and M. Ernzerhof, *Phys. Rev. Lett.*, 1996, **77**, 3865–3868.
126 Y. Zhang and W. Yang, *Phys. Rev. Lett.*, 1998, **80**, 890–890.
127 S. Grimme, J. Antony, S. Ehrlich and H. Krieg, *The Journal of Chemical Physics*, 2010, **132**, 154104.
128 S. Grimme, S. Ehrlich and L. Goerigk, *Journal of Computational Chemistry*, 2011, **32**, 1456–1465.
129 A. Cabrera-Ramírez, D. J. Arismendi-Arrieta, Á. Valdés and R. Prosmiti, *ChemPhysChem*, 2021, **22**, 359–369.
130 G. Kresse and D. Joubert, *Phys. Rev. B*, 1999, **59**, 1758–1775.
131 A. Lenz and L. Ojamäe, *J. Phys. Chem. A*, 2011, **115**, 6169–6176.
132 V. Wang, N. Xu, J.-C. Liu, G. Tang and W.-T. Geng, *Computer Physics Communications*, 2021, **267**, 108033.
133 F. Neese, *WIREs Computational Molecular Science*, 2012, **2**, 73–78.
134 F. Neese, *WIREs Computational Molecular Science*, 2018, **8**, e1327.
135 V. Barone, *The Journal of Chemical Physics*, 1994, **101**, 6834–6838.
136 N. Rega, M. Cossi and V. Barone, *The Journal of Chemical Physics*, 1996, **105**, 11060–11067.
137 R. Ditchfield, *Molecular Physics*, 1974, **27**, 789–807.
138 K. Wolinski, J. F. Hinton and P. Pulay, *J. Am. Chem. Soc.*, 1990, **112**, 8251–8260.
139 A. D. Becke, *The Journal of Chemical Physics*, 1993, **98**, 5648–5652.
140 C. Lee, W. Yang and R. G. Parr, *Phys. Rev. B*, 1988, **37**, 785–789.
141 S. H. Vosko, L. Wilk and M. Nusair, *Can. J. Phys.*, 1980, **58**, 1200–1211.
142 P. J. Stephens, F. J. Devlin, C. F. Chabalowski and M. J. Frisch, *J. Phys. Chem.*, 1994, **98**, 11623–11627.

This journal is © The Royal Society of Chemistry 2023

Please do not adjust margins